

QUASI-OPTICAL BESSEL RESONATOR

Y. Z. Yu and W. B. Dou [†]

State Key Lab of Millimeter Waves
Southeast University
Nanjing, Jiangsu 210096, China

Abstract—In this paper, a quasi-optical Bessel resonator (QOBR) for generating approximations to Bessel-type modes at millimeter wavelengths has been designed and analyzed. A design approach is based on the quasi-optical techniques. In order to analyze the designed QOBR rigorously, a new method based on iterative Stratton-Chu formula (ISCF) is developed from the classical Fox-Li algorithm and its validity is demonstrated. Numerical results reveal that at the output plane the intensity distributions of the Bessel-type modes of the designed QOBR are modulated by a bell-shaped envelope, and their phase patterns have a block-shaped profile except slight distortion on the edges of the output plane due to aperture diffraction. The effect of varying the parameters of the designed QOBR on the relevant output characteristics is also examined in our study.

1. INTRODUCTION

Bessel beams, introduced firstly by Durnin and co-workers in 1987 [1, 2], have attracted much attention and been investigated intensively over more than twenty years, owing to their potential applications in physics, chemistry, biology, and engineering. Numerous approaches to generate pseudo Bessel beams have been suggested, which can be sorted roughly into two classes [3–5], i.e., passive and active schemes. The first class uses the spatial filter to transform an incident beam into an approximation to Bessel beam, such as narrow annular slit [2], computer-generated holograms (CGHs) [6–8], Fabry-Perot cavity [9], optical refracting systems [10], axicon [11–14] and diffractive phase elements (DPEs) [15–17]. The other class

Corresponding author: Y. Z. Yu (yuyanzhong059368@gmail.com).

[†] Y. Z. Yu is also with School of Science, Quanzhou Normal University, Quanzhou, Fujian 362000, China.

is formed by methods relying on a resonator frame to produce the Bessel-type modes. For example, resonators with annular intracavity elements [18], output mirrors having annular apertures [19], phase-conjugating mirrors [20], and axicon-based resonators [3–5, 21–24]. When compared with the passive schemes, the active have the following advantages [5, 23]: They generate the Bessel-type modes directly from the resonators, omitting the external filter elements and resulting in high-output-power Bessel beams; another is the possibility of realizing intracavity frequency conversion of Bessel beams.

However, in millimeter range, only the passive schemes for producing Bessel beams have been proposed and studied currently. Examples can be found in [7, 8, 12–16]. To our knowledge, no active schemes have been reported at these wavebands as yet. Accordingly, the purpose of the present paper is to design and analyze the QOBR that support approximations to Bessel-type modes at millimeter wavebands. The configuration of the QOBR is constructed by the quasi-optical techniques. To precisely calculate the resonant modes of the designed QOBR at millimeter wavebands, a more rigorous method (ISCF method), based on the Stratton-Chu diffraction integral formula, is developed from the famous Fox-Li iterative algorithm [25]. The demonstration of its validity is made by comparing the computational results obtained by the ISCF and Fox-Li algorithms. It is indicated from the numerical simulation results that at the output plane the modulated intensities in the Bessel-type modes of the designed QOBR seem like a bell-shaped contour; however, aside from little deformation on the edges of the output mirror because of aperture diffraction, the phase patterns of them show a block-shaped outline. We have also investigated the influence of manufacture errors of the designed QOBR on the output characteristics.

The rest of the present paper is organized as follows. The design of the QOBR is described in Section 2. The ISCF method is developed and its validity is verified in Section 3 and Section 4, respectively. The numerical results are presented in Section 5. In the last Section 6, a brief summary is made.

2. QOBR DESIGN

In contrast to structures of the resonators proposed in [18–20], the axicon-based resonator is probably the most attractive one because of its simplicity and high conversion efficiency [5]. It is known that an axicon converts an incident plane wave into an approximation to Bessel beam [11–14], located within the interference zone ECFD, as depicted in Fig. 1(a). The field distribution of the l th-order Bessel beam in the

cylindrical coordinates system is written as:

$$U_l(\rho, \varphi, z) = U_0 J_l(k_{\perp} \rho) \exp(jk_z z) \exp(jl\varphi) \quad (1)$$

where U_0 is a constant, J_l denotes the l th-order Bessel function of the first kind, $\rho^2 = x^2 + y^2$, $k_{\perp}^2 + k_z^2 = (2\pi/\lambda)^2$, k_{\perp} and k_z are the radial and longitudinal wave numbers, respectively. λ is the free space wavelength. Now, assuming that a reflective mirror is embedded at the plane CD , the Bessel beam would be reflected upon itself. If the base plane AB of the axicon is backed by a perfectly reflecting plane mirror, whereas the output mirror CD is only the partially reflective, then the Bessel resonator can be constructed and the output beam can be obtained from the plane CD , see Fig. 1(b). In practice, the refractive axicon with the perfectly reflecting base can be superseded by a reflective axicon, as shown in Fig. 1(c), leading to an alternative but equivalent realization of the Bessel resonator [3]. In such case the relation between

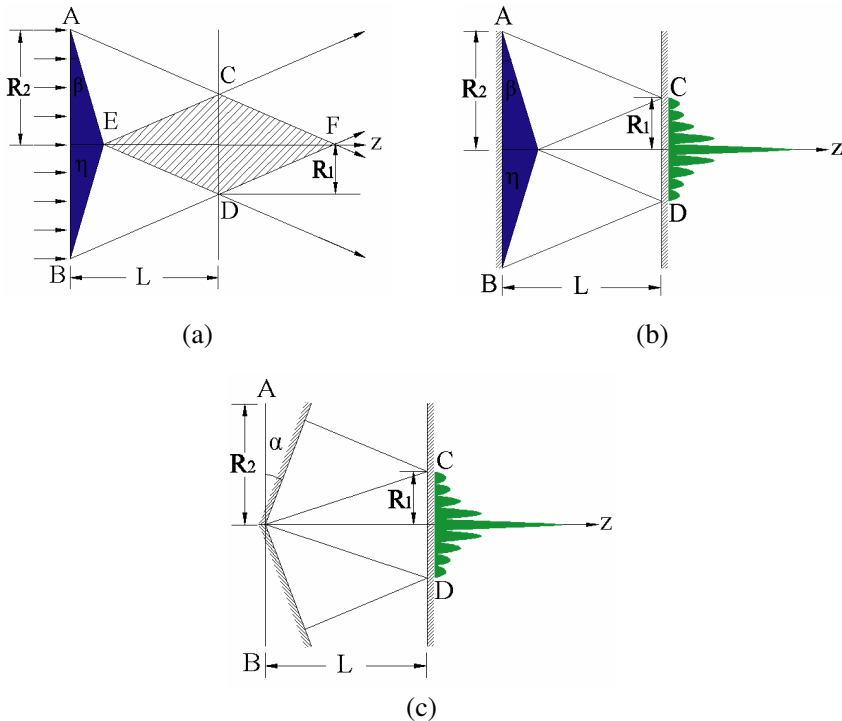


Figure 1. Design of the QOBRs. (a) An incident plane wave is converted by an axicon into a conical wave (Hankel wave); (b) the QOBR with a refractive axicon; (c) the QOBR with a reflective axicon.

the conical angle α of the reflective axicon and the apex angle β of the refractive axicon is expressed by $\alpha = \arcsin(\eta \sin(\beta)) - \beta$, where η is the refractive index. The configuration in Fig. 1(c) is more suitable for standing high power in comparison with that in Fig. 1(b), since the reflective axicon can be made of perfect conductor rather than the dielectric, which is used to make the refractive one. For this reason, the structure illustrated in Fig. 1(c) is adopted to form the QOBR in our design. It has been shown that the gain in the cavity volume is maximized if distance L between the axicon and the plane mirror is chosen to be [21]

$$L = \frac{R_2}{2 \tan \alpha} \quad (2)$$

where R_2 is the aperture radius of the refractive or reflective axicon and $R_2 = 2R_1$.

3. DEVELOPMENT OF ANALYSIS METHOD

The famous Fox-Li algorithm, proposed by Fox and Li in 1960 [25], has been used successfully to analyze the resonant modes in optical cavities. This method, based on the Kirchhoff scalar formula for diffraction, is permissible and justifiable, if the numerical aperture (NA) is rationally small; the Fresnel number is very large; and the incident radiation is unpolarized [26]. Looseness of any of these three assumptions invalidates the Kirchhoff analysis. In general, the above requirements are easily satisfied in optical region and the Fox-Li algorithm can thus be applied reliably. However, it is not quite fit for analysis the resonator in the spectrum of millimeter rang, as all constraints mentioned above are usually no longer satisfied simultaneously. Therefore, to rigorously compute the resonant modes of the designed QOBR at millimeter wavelengths, the ISCF method is developed in our analysis. It applies the vector form of the Stratton-Chu formula for diffraction, rather than the scalar form of the Kirchhoff formula for diffraction, to compute the electromagnetic fields in the cavity. The magnetic field component \vec{H} of the Stratton-Chu diffraction integral formula is given by [27]

$$\begin{aligned} \vec{H}(\vec{r}) = \int_{S'} \left\{ j\omega\epsilon \left[\vec{n} \times \vec{E}(\vec{r}') \right] G_0(\vec{r}, \vec{r}') + \left[\vec{n} \times \vec{H}(\vec{r}') \right] \right. \\ \left. \times \nabla' G_0(\vec{r}, \vec{r}') + \left[\vec{n} \cdot \vec{H}(\vec{r}') \right] \nabla' G_0(\vec{r}, \vec{r}') \right\} dS' \end{aligned} \quad (3)$$

where \vec{r} and \vec{r}' represent an arbitrary observation point in the far region and an source point on the integral surface S' , respectively;

unit vector \vec{n} is the outer normal of the integral surface S' ; ω and ε are the angular frequency and the permittivity, respectively. $G_0(\vec{r}, \vec{r}')$ is the free-space Green's function given by

$$G_0(\vec{r}, \vec{r}') = \exp(jk|\vec{r} - \vec{r}'|) / 4\pi|\vec{r} - \vec{r}'| \quad (4)$$

for the three-dimensional (3-D) problem and by

$$G_0(\vec{r}, \vec{r}') = -\frac{j}{4}H_0^{(2)}(k|\vec{r} - \vec{r}'|) \quad (5)$$

for the 2-D problem. $H_0^{(2)}$ is the zero-order Hankel function of the second kind and k is the wave number in the free space. When Eq. (3) is employed to calculate the field reflected by a perfectly conducting surface, the boundary conditions: $\vec{n} \times \vec{E} = 0$ and $\vec{n} \cdot \mu \vec{H} = 0$ should be imposed on it. In such case, Eq. (3) is reduced as

$$\begin{aligned} \vec{H}(\vec{r}) &= \int_{S'} \left\{ \left[\vec{n} \times \vec{H}(\vec{r}') \right] \times \nabla' G_0(\vec{r}, \vec{r}') \right\} dS' \\ &= \int_{S'} \left\{ \left[2\vec{n} \times \vec{H}_i(\vec{r}') \right] \times \nabla' G_0(\vec{r}, \vec{r}') \right\} dS' \end{aligned} \quad (6)$$

where the fact that $\vec{n} \times \vec{H}(\vec{r}') = 2\vec{n} \times \vec{H}_i(\vec{r}')$ on the perfectly conducting surface is considered, \vec{H}_i denotes the incident magnetic field vector.

Now, let us describe the ISCF algorithm. To understand easily and calculate conveniently, the round-trip propagation inside the cavity is divided into two one-way transits, as illustrated schematically in Fig. 2. In the first transit, namely, the propagation of the electromagnetic wave from the mirror M_1 to mirror M_2 , according to Eq. (6) the diffracted field $\vec{H}_2(\vec{r}_2)$ at the M_2 can be written as

$$\vec{H}_2(\vec{r}_2) = \int_{S_1} \left\{ \left[2\vec{n}_1 \times \vec{H}_1(\vec{r}_1) \right] \times \nabla' G_0(\vec{r}_2, \vec{r}_1) \right\} dS_1 \quad (7)$$

Similar expression can be obtained for the diffracted field $\vec{H}_3(\vec{r}_1)$ at the M_1 in the second transit

$$\vec{H}_3(\vec{r}_1) = \int_{S_2} \left\{ \left[2\vec{n}_2 \times \vec{H}_2(\vec{r}_2) \right] \times \nabla' G_0(\vec{r}_1, \vec{r}_2) \right\} dS_2 \quad (8)$$

The various symbols are defined in Fig. 2. According to the self-consistency condition, we can obtain the following relation after transiting m times and approaching a steady state

$$\vec{H}_{m+1} = \frac{1}{\gamma} \vec{H}_{m-1} \quad (9)$$

where \vec{H} represents the eigenfield distribution at the M_1 or M_2 ; γ is the complex eigenvalue independent of the position coordinate, which defines the fractional power loss per round-trip

$$\delta = 1 - \left| \frac{1}{\gamma} \right|^2 \quad (10)$$

and the additional phase shift per round-trip

$$\Phi = \arg \frac{1}{\gamma} \quad (11)$$

The procedure of implementing the ISCF algorithm is summarized as follows. The first step of the ISCF algorithm is to generate an initial field distribution $\vec{H}_1(\vec{r}_1)$ at the M_1 . General speaking, it can be assumed arbitrarily. Secondly, substitution of $\vec{H}_1(\vec{r}_1)$ into Eq. (7) yields $\vec{H}_2(\vec{r}_2)$. Then, normalizing $\vec{H}_2(\vec{r}_2)$, i.e., $|\vec{H}_2(\vec{r}_2)|_{\max} = 1$, and substituting it into Eq. (8), we get $\vec{H}_3(\vec{r}_1)$. This computation process is repeated until the relative field distribution reaches a steady state, that is, satisfies Eq. (9). We regard this field distribution as an iterative normal mode of the resonator [25].

4. DEMONSTRATION THE VALIDITY OF THE ISCF METHOD

It is worth pointing out that the ISCF method described in Section 3 is not only suitable for analysis the resonator at millimeter wavebands but also in the optical region. In other words, the applicable range of the ISCF method is wider than the Fox-Li approach. Therefore, the validity of the ISCF method can be demonstrated by comparing the analysis results obtained by the ISCF and Fox-Li algorithms. The cavity, used to analyze comparison, originated from [25], and its configuration is composed of two parallel infinite strip mirrors, which is a 2-D problem. The dimension of the strip mirrors is $R = 25\lambda$ and the cavity length is $L = 100\lambda$. Assuming an initial excitation $\vec{H}_1(x_1) = \vec{y}$ and employing Eqs. (7) and (8) for the computation, the

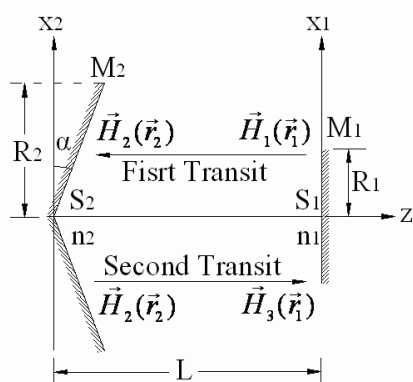


Figure 2. A computational model for the QOBR. A propagating wave is reflected back and forth by two mirrors; and a round-trip is divided into two one-way transits. The inner surfaces of the M_1 and M_2 are denoted by S_1 and S_2 , respectively. n_1 and n_2 are the normal of the S_1 and S_2 , respectively. R_1 and R_2 represent the aperture radius of the M_1 and M_2 , respectively; L is the cavity length and α is the conical angle of the M_2 . H_{m+1} represents the filed distribution of the m th-time transit.

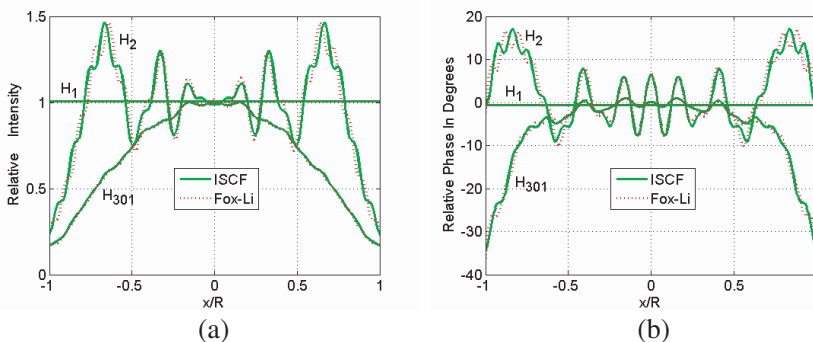


Figure 3. Comparison of the results obtained by the ISCF and Fox_Li algorithms. (a) Relative intensity distributions of the field for the infinite strip mirrors; (b) relative phase distributions.

steady state can be reached after three hundred transits. The intensity and phase distributions for the \vec{H}_1 , \vec{H}_2 , \vec{H}_{301} , calculated by the ISCF and Fox-Li algorithms, are plotted respectively in Figs. 3(a) and 3(b). It can be seen obviously from Fig. 3 that not only the intensity but also the phase curves exhibit excellent agreements. Additionally, the

power loss and phase shift per transit gotten by the ISCF algorithm are 0.6679% and 1.565° , respectively, which are almost the same as the results of 0.6673% and 1.578° , obtained by the Fox-Li approach in our calculation. Moreover, these results are very close to the values of 0.688% and 1.59° computed by Fox and Li in [25]. These numerical results serve to validate the ISCF method. Now, it can be employed confidently to analyze the designed QOBR in millimeter range.

5. NUMERICAL ANALYSIS

Recently, a quasi-optical open resonator supporting Gaussian modes has been designed and employed to measure dielectric parameters at millimeter wavebands in our group [28–30]. The geometrical parameters for the designed QOBR are hence related to this Gaussian resonator: aperture size of the reflective axicon $R_2 = 85$ mm, cavity length $L = 103.1$ mm, and wavelength $\lambda = 8$ mm. And then the aperture radius of the output mirror is $R_1 = R_2/2 = 42.5$ mm. From Eq. (2), the value for the conical angel α is computed to be approximately $\alpha = 22.4^\circ$. The rotational symmetry of the QOBR enables us to reduce a 3-D calculation to a 2-D one, which can save computational resources significantly. Using an initial excitation of a uniform plane wave at the M_1 , i.e., $\vec{H}_1(x_1) = \vec{y}$, and applying Eqs. (7) and (8) for the iterative calculation, the fundamental mode of the

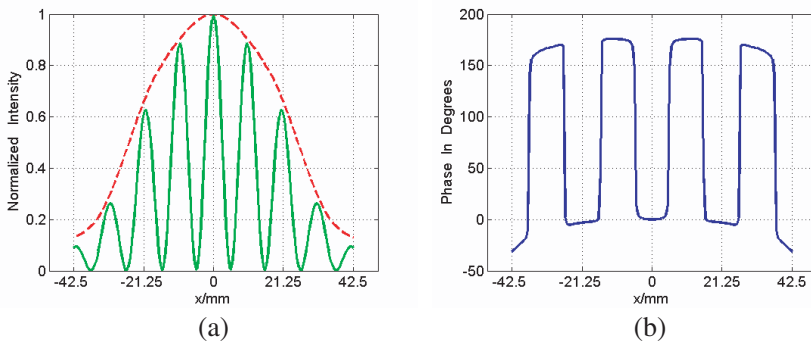


Figure 4. The intensity and phase distributions of the dominant Bessel-type mode for the designed QOBR at the output mirror. (a) The intensity profile is modulated by a bell-shaped envelope (broken red line); (b) the phase pattern has a block-shaped profile excluding tiny aberration on the edges of the output mirror; moreover, it is even-symmetric about z -axis.

designed QOBR can be readily acquired after three hundred transits. Fig. 4 shows the intensity and phase distributions of the field at the M_1 . It can be observed clearly from Fig. 4(a) that the intensity profile of the dominant Bessel-type mode is modulated by a bell-shaped envelope (broken red line -), which corresponds to the lowest-order mode of a cavity constructed by two parallel plane mirrors with aperture radius R_1 and separated by length $2L$. The modulation resulted from the fact that within the QOBR each plane wave component of the Hankel wave will be suffered from reflection by two parallel plane mirrors [see Fig. 1(c)], having radius R_1 and cavity length $\sim 2L$ [21, 22]. Moreover, this modulation in a Bessel intensity profile is inevitable owing to the finite extent of elements in a real QOBR. The phase pattern of an ideal Bessel beam has a block-shaped profile. However, the phase distribution of the fundamental Bessel-type mode depicted in Fig. 4(b) exhibits little aberration due to diffraction on the edges of the aperture of the M_1 . In addition, from Eqs. (10) and (11), the power loss and phase shift per round-trip is computed, yielding $\delta = 5.49\%$ and $\Phi = 60.81^\circ$, respectively.

If an initial field at the M_1 is preset as: $\vec{H}_1(x_1 > 0) = \vec{y}$ but $\vec{H}_1(x_1 < 0) = -\vec{y}$, the high-order Bessel-type mode can be excited. Its intensity and phase distributions at the M_1 are plotted in Fig. 5. The normalized intensity distribution is not unit one but zero at the

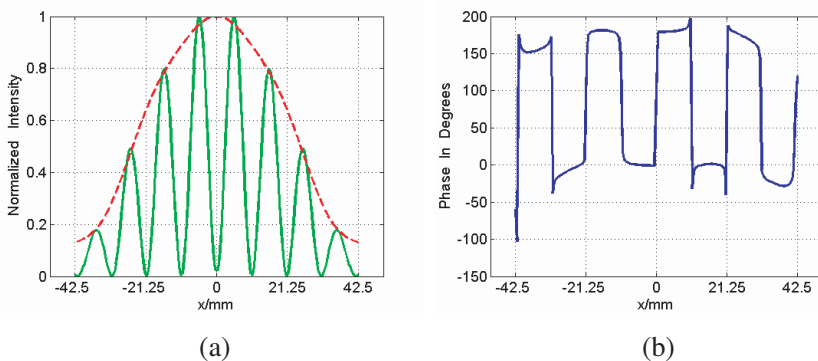


Figure 5. The intensity and phase distributions of the high-order Bessel-type mode for the designed QOBR at the output mirror. (a) The intensity distribution has a zero at the center, and its profile is still modulated by a bell-shaped envelope (broken red line); (b) the phase pattern shows a block-shaped frame; however, it is odd-symmetric about z -axis.

center of the M_1 , due to the existence of phase singularity there. The modulation in the intensity profile of high-order Bessel-type mode is the same as that of the lowest-order one. The phase distribution of the high-order mode still displays a block-like frame, but it is odd-symmetric about z -axis, which is different from that of the lowest-order one with an even symmetry about z -axis. In the same way, the values of $\delta = 7.85\%$ and $\Phi = 60.83^\circ$ can be obtained. As expected, they are a little larger than those of the dominant mode, correspondingly.

The manufacture errors of the designed QOBR are unavoidable. Therefore, it is great helpful to examine the influence of varying the parameters of the designed QOBR on the output characteristics including the intensity and phase distributions, power loss and phase shift per round-trip. Provided that only the aperture radii of two elements have an error, i.e., $R_1 = 42.5 \pm 1$ mm and $R_2 = 85 \pm 2$ mm,

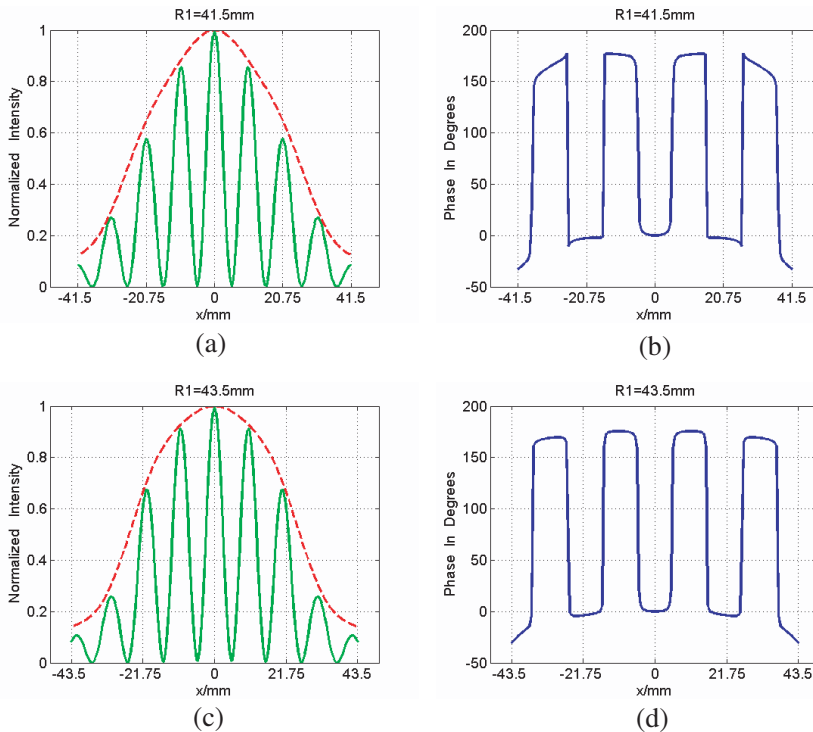


Figure 6. The influence of changing the radii of two elements on the output distributions. The intensity and phase distributions of the fundamental mode for (a), (b) $R_1 = 41.5$ mm and (c), (d) $R_1 = 43.5$ mm.

the fundamental modes can be evaluated, respectively. And their intensity and phase distributions at the M_1 are illustrated in Fig. 6. The influence of changing the conical angle of $\alpha = 22.4 \pm 0.5^\circ$ on the output distributions are shown in Fig. 7. From Figs. 6 and 7, it can be seen clearly that their distributions agree with those represented in Fig. 4, correspondingly. This means that Bessel-type modes are still maintained well within the designed QOBR, although there exist machining errors of the radius and conical angle. The power losses and phase shifts per round-trip are summed up in Table 1. From Table 1, we can see that the power losses of the fundamental modes are close to the value of 5.49%; however, the phase shifts are more sensitive to conical angle errors than aperture radius errors.

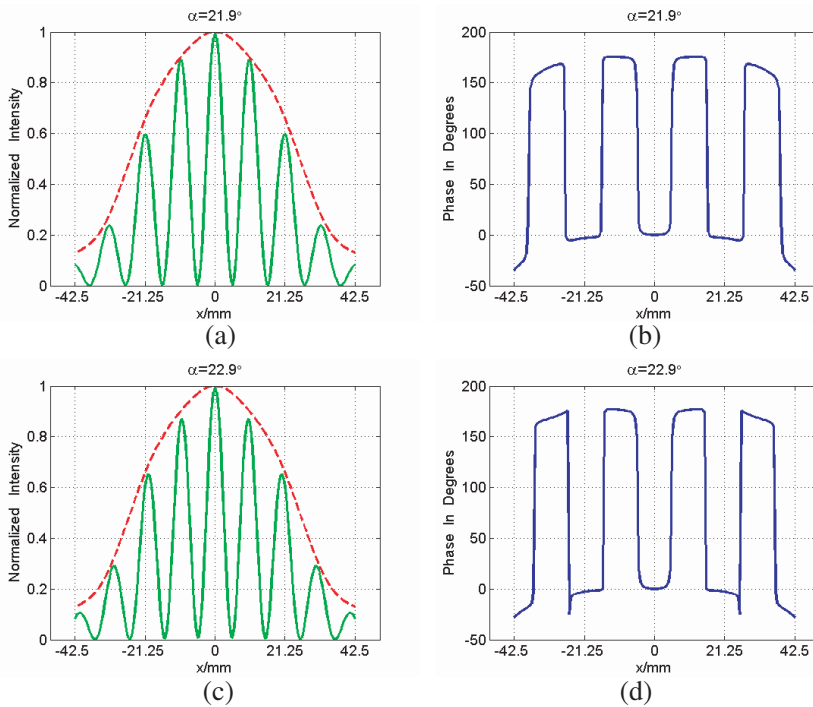


Figure 7. The effect of varying the conical angle of the reflective axicon on the output distributions. The intensity and phase distributions for (a), (b) $\alpha = 21.9^\circ$ and (c), (d) $\alpha = 22.9^\circ$.

Table 1. The power losses and phase shifts of the dominant Bessel-type modes.

Aperture radius R_1 (mm)	Conical angle α (°)	power loss δ (%)	phase shift Φ (°)
42.5	22.4	5.49	60.81
42.5 - 1	22.4	6.14	61.14
42.5 + 1	22.4	4.85	60.55
42.5	22.4 - 0.5	5.80	30.56
42.5	22.4 + 0.5	5.13	91.79

6. SUMMARY

On the basis of quasi-optical techniques and the developed iterative method (ISCF method), the QOBR at millimeter wavelengths is designed and its resonant modes is analyzed. The processing errors of the designed QOBR are also considered. Similar to the practical applications of a quasi-optical open resonator sustaining Gaussian modes [31–38], we believe that the designed QOBR, besides the production of Bessel-type modes, have many promising applications in millimeter range, such as frequency measurement, spectrum analysis, transmission characteristic research, power combination, and dielectric parameter measurement. Therefore, the study of the QOBR in these spectrum ranges has important practical significance.

ACKNOWLEDGMENT

This work is supported by NSFC under grant 60621002, and the Key Project of Quanzhou City Science and Technology Program (No. 2008G13).

REFERENCES

1. Durnin, J., “Exact solutions for nondiffracting beams. I. The scalar theory,” *J. Opt. Soc. Am. A*, Vol. 4, No. 4, 651–654, 1987.
2. Durnin, J., J. J. Miceli, Jr., and J. H. Eberly, “Diffraction-free beams,” *Phys. Rev. Lett.*, Vol. 58, No. 15, 1499–1501, 1987.
3. Muys, P. and E. Vandamme, “Direct generation of Bessel beams,” *Appl. Opt.*, Vol. 41, No. 30, 6375–6379, 2002.
4. Hernandez-Aranda, R. I., S. Chavez-Cerda, and J. C. Gutierrez-Vega, “Theory of the unstable Bessel resonator,” *J. Opt. Soc. Am. A*, Vol. 22, No. 9, 1909–1917, 2005.

5. Wu, F., Y. Chen, and D. Guo, "Nanosecond pulsed Bessel-Gauss beam generated directly from a Nd: YAG axicon-based resonator," *Appl. Opt.*, Vol. 46, No. 22, 4943–4947, 2007.
6. Vasara, V., J. Turunen, and A. T. Friberg, "Realization of general nondiffracting beams with computer-generated holograms," *J. Opt. Soc. Am. A*, Vol. 6, No. 11, 1748–1754, 1989.
7. Salo, J., J. Meltaus, E. Noponen, et al., "Millimeter-wave Bessel beams using computer holograms," *Electron. Lett.*, Vol. 37, No. 13, 834–835, 2001.
8. Meltaus, J., J. Salo, E. Noponen, et al., "Millimeter-wave beam shaping using holograms," *IEEE Trans. Microwave Theory Tech.*, Vol. 51, No. 4, 1274–1279, 2003.
9. Cox, A. J. and D. C. Dibble, "Nondiffracting beam from a spatially filtered Fabry-Perot resonator," *J. Opt. Soc. Am. A*, Vol. 9, No. 2, 282–286, 1992.
10. Thewes, K., M. A. Karim, and A. A. S. Awwal, "Diffraction free beam generation using refracting systems," *Opt. Laser Technol.*, Vol. 23, No. 2, 105–108, 1991.
11. Herman, R. M. and T. A. Wiggins, "Production and uses of diffractionless beams," *J. Opt. Soc. Am. A*, Vol. 8, No. 6, 932–942, 1991.
12. Monk, S., J. Arlt, D. A. Robertson, et al., "The generation of Bessel beams at millimetre-wave frequencies by use of an axicon," *Opt. Commun.*, Vol. 170, 213–215, 1999.
13. Yu, Y. Z. and W. B. Dou, "Properties of approximate Bessel beams at millimeter wavelengths generated by fractal conical lens," *Progress In Electromagnetics Research*, PIER 87, 105–115, 2008.
14. Yu, Y. Z. and W. B. Dou, "Generation of pseudo-Bessel beams at THz frequencies by use of binary axicons," *Opt. Express*, Vol. 17, No. 2, 888–893, 2009.
15. Yu, Y. Z. and W. B. Dou, "Generation of Bessel beams at mm- and sub mm-wavelengths by binary optical elements," *Int. J. Infrared Milli. Waves*, Vol. 29, No. 7, 693–703, 2008.
16. Yu, Y. Z. and W. B. Dou, "Generation of mm- and sub mm-wave Bessel beams using DOE's Designed by BOR-FDTD method and MGA," *J. Infrared Milli. Terahz Waves*, Vol. 30, No. 2, 172–182, 2009.
17. Cong, W. X., N. X. Chen, and B. Y. Gu, "Generation of nondiffracting beams by diffractive phase elements," *J. Opt. Soc. Am. A*, Vol. 15, No. 9, 2362–2364, 1998.

18. Durnin, J. and J. H. Eberly, "Diffraction free arrangement," U.S. Patent 4,887,885, December 19, 1989.
19. Uehara, K. and H. Kikuchi, "Generation of nearly diffraction-free laser beams," *Appl. Phys. B*, Vol. 48, No. 2, 125–129, 1989.
20. Pääkkönen, P. and J. Turunen, "Resonators with Bessel-Gauss modes," *Opt. Commun.*, Vol. 156, 359–366, 1998.
21. Rogel-Salazar, J., G. H. C. New, and S. Chávez-Cerda, "Bessel-Gauss beam optical resonator," *Opt. Commun.*, Vol. 190, 117–122, 2001.
22. Tsangaris, C. L., G. H. C. New, and J. Rogel-Salazar, "Unstable Bessel beam resonator," *Opt. Commun.*, Vol. 223, 233–238, 2003.
23. Khilo, A. N., E. G. Katranji, and A. A. Ryzhevich, "Axicon-based Bessel resonator: Analytical description and experiment," *J. Opt. Soc. Am. A*, Vol. 18, No. 8, 1986–1992, 2001.
24. Gutiérrez-Vega, J. C., R. Rodríguez-Masegosa, and S. Chávez-Cerda, "Bessel-Gauss resonator with spherical output mirror: geometrical and wave-optics analysis," *J. Opt. Soc. Am. A*, Vol. 20, No. 11, 2113–2122, 2003.
25. Fox, A. G. and T. Li, "Resonant modes in a maser interferometer," *Bell Syst. Tech. J.*, Vol. 40, 453–488, 1961.
26. Hsu, W. and R. Barakat, "Stratton-Chu vectorial diffraction of electromagnetic fields by apertures with application to small-Fresnel-number systems," *J. Opt. Soc. Am. A*, Vol. 11, No. 2, 623–629, 1994.
27. Stratton, J. A., *Electromagnetic Theory*, McGraw-Hill, New York, 1941.
28. Gui, Y. F., W. B. Dou, K. Yin, and P. G. Su, "Automated and precise dielectric measurement systems at millimeter wavelengths using open resonator technique," *2008 Global Symposium on Millimeter Waves*, 66–69, 2008.
29. Gui, Y. F., W. B. Dou, K. Yin, and P. G. Su, "Open resonator system for automatic and precise dielectric measurement at millimeter wavelengths," *Int. J. Infrared Milli. Waves*, Vol. 29, No. 8, 782–791, 2008.
30. Gui, Y. F., W. B. Dou, K. Yin, and P. G. Su, "The improvement of open resonator technique for dielectric measurement at millimeter wavelengths," *IET Microwaves, Antennas and Propagation*, Accepted.
31. Asitya, S. and T. Naveen, "An automated open resonator technique for measurement of extinction cross-section of single falling water drops over X-band," *Progress In Electromagnetics*

- Research*, PIER 8, 161–171, 1994.
32. Perov, A. O., Y. K. Sirenko, and N. P. Yashina, “Periodic open resonators: Peculiarities of pulse scattering and spectral features,” *Progress In Electromagnetics Research*, PIER 46, 33–75, 2004.
 33. Velychko, L. G. and Y. K. Sirenko, “Time-domain analysis of open resonators analytical grounds,” *Progress In Electromagnetics Research*, PIER 61, 1–26, 2006.
 34. Geyi, W., “Time-domain theory of metal cavity resonator,” *Progress In Electromagnetics Research*, PIER 78, 219–253, 2008.
 35. Saliminejad, R. and M. R. Ghafouri Fard, “A novel and accurate method for designing dielectric resonator filter,” *Progress In Electromagnetics Research B*, Vol. 8, 293–306, 2008.
 36. Shin, D. H. H. and T. Itoh, “A note on radiation loss of zeroth order resonators,” *Progress In Electromagnetics Research C*, Vol. 2, 109–116, 2008.
 37. Maab, H. and Q. A. Naqvi, “Fractional rectangular cavity resonator,” *Progress In Electromagnetics Research B*, Vol. 9, 69–82, 2008.
 38. Malekabadi, S. A., M. H. Neshati, and J. Rashed-Mohassel, “Circular polarized dielectric resonator antennas using a single probe feed,” *Progress In Electromagnetics Research C*, Vol. 3, 81–94, 2008.